SCIENTIFIC REPORTS

OPEN

SUBJECT AREAS:
ELECTRONIC DEVICES
SUPERCONDUCTING DEVICES

Received
11 April 2014

Accepted
30 June 2014

Published
18 July 2014

Correspondence and requests for materials should be addressed to K.M. (makise@nict.go.jp)

Microstructural analysis and Transport Properties of MoO and MoC nanostructures prepared by focused electron beam-induced deposition

Kazumasa Makise[1], Kazutaka Mitsuishi[2], Masayuki Shimojo[3] & Bunju Shinozaki[4]

[1]Advanced ICT Research Institute, National Institute of Information and Communications Technology, 588-2 Iwaoka, Kobe, Hyogo 651-2492, Japan, [2]Surface Physics and Structure Unit, National Institute for Materials Science, 3-13 Sakura, Tsukuba 305-0003, Japan, [3]Department of Materials Science and Engineering, Shibaura Institute of Technology, 3-7-5 Toyosu, Koto-ku, Tokyo 135-8548, Japan, [4]Department of Physics, Kyushu University, 6-10-1 Hakozaki, Higashiku, Fukuoka 812-8581, Japan.

By electron-beam-induced deposition, we have succeeded in the direct fabrication of nanowires of molybdenum oxide (MoO_x) and molybdenum carbide (MoC) on a SiO_2 substrate set in a scanning electron microscope. In order to prepare MoO_x specimens of high purity, a precursor gas of molybdenum hexacarbonyl [$Mo(CO)_6$] is used, mixed with oxygen gas. On the other hand, MoC is grown by mixing H_2O gas with the precursor gas. The electrical transport properties of the nanowires are investigated by the DC four-terminal method. A highly resistive MoO_x nanowire prepared from an as-deposited specimen by annealing in air shows nonlinear current-voltage characteristics and a high photoconductivity. The resistivity ρ of an as-deposited amorphous MoC (a-MoC) nanowire takes its maximum at a temperature $T \approx 10$ K and decreases to ≈ 0 with decreasing temperature. This behavior of $\rho(T)$ indicates the possible occurrence of superconductivity in a-MoC nanowires. The characteristic of $\rho(T)$ below the superconducting transition temperature $T_c \approx 4$ K can be well explained by the quantum phase-slip model with a coherence length $\xi(0) \approx 8$ nm at $T=0$.

The application of nanostructure materials in electronic or optoelectronic devices is one of the major focuses in recent nanoscience research. Nanowire and nanotube devices are particularly important from the viewpoint of nanosize function. These devices are applied in single-electron transistors, field-effect transistors, and metal-semiconductor junctions. Growth of the fabrication technology for nanostructures has already resulted in the development of several special devices using quantum dots and nanowires[1–3].

The conventional method of fabricating nanodots, nanowires and nanorods cannot be used to directly deposit materials on a small substrate. Recently, technology using focused ion or electron beams has attracted interest from the viewpoint of its application to the direct growth of nanostructures for use in electronics and optoelectronics. Methods of ion-beam-induced deposition (IBID) and electron-beam-induced deposition (EBID) are suitable for the fabrication of structures with different sizes on the nanometer scale[4–8]. In addition, these methods require no cumbersome steps, namely, the use of masks, photoresist or electron beam lithography, and lift-off procedures. The IBID method has been successfully used for the fabrication of complicated structures such as actuators and manipulators on a micrometer scale. On the other hand, EBID using various precursors has been carried out for various materials, e.g, W, C, Fe, Pt and Au[9–13]. In addition to the use of these common metals to prepare semiconducting and superconducting materials with nanoscale structures, EBID is superior to IBID for the following reasons: 1) As the probe of the focused electron beam of the field emission gun is smaller than that of the focused ion beam, EBID is suitable for deposition on a small area. Therefore, three-dimensional nanostructures can be fabricated on very small areas such as the top of the tungsten STM tip. 2) IBID damages predeposited electrodes and even the specimen on substrates by Ga ion irradiation, whereas EBID markedly reduces the risk of this damage due to electron impingement. 3) Superconducting or semiconducting nanowires prepared by EBID have none of the Ga contaminants produced by IBID on the substrate.

Molybdenum oxide (MoO_x) is an interesting material and thus has been investigated for various applications such as gas sensors[14], catalysts[15] and metal-gate applications[16]. From the present measurements of the resistivity of

(Mo-based) nanowires fabricated on Pt/Ti electrodes, it is found that highly resistive MoO_x nanowires show photoconducting behavior, suggesting their potential as Schottky barrier diodes. This result enables us to fabricate nanoscale devices of molybdenum systems with controlled size and position. To our knowledge, there has been no study of the superconducting properties of metallic molybdenum carbide (MoC) nanowires fabricated by EBID as in the present investigation.

In this letter, we report on the results of on-demand fabrication by EBID for nanowires of MoO_x, Mo and MoC as well as on the transport properties of these nanowires.

Specimen preparation and experimental procedure. Nanowires were grown using a 30 KV field emission gun scanning electron microscope (SEM; JEOL JSM-7800UHV) with a custom-built gas injection system. Using $Mo(CO)_6$ gas as the precursor, nanowires were prepared by deposition on a SiO_2 substrate with Pt/Ti electrodes of low contact resistance.

To prepare MoO_x, we introduced the precursor gas $Mo(CO)_6$ mixed with oxygen gas through the nozzle into a high-vacuum chamber. MoC nanowires were prepared using the same EBID deposition system by introducing a mixed gas of $Mo(CO)_6$ and H_2O. The partial pressures of these gases were carefully controlled using leak valves. During the deposition, the background pressure of the chamber was kept at about 4×10^{-5} Pa. The gas injection system was described in detail elsewhere.

Electrical properties, current–voltage (*I-V*) characteristics and the temperature *T* and magnetic field *H* dependences of the resistivity ρ have been investigated by a standard DC two- or four-terminal technique using a Keithley 6221 current source, a 2400 source measurement unit and a nanovoltmeter 2182. An external magnetic field was applied perpendicularly to the current direction through nanowires with a superconducting solenoid set inside the Dewar assembly. Lead wires of Au were connected to the surface of Pt/Ti electrode pads with Ag paste and indium solder. It was confirmed that the ohmic contact was held between the electrodes and the specimens during the *I-V* measurement in the bias voltage range of -10 V to $+10$ V. Light power was measured using an optical power meter (Advantest TQ 8215). The white light of the emitted diode was used as the light source to observe photoconductance as a function of turning the light on and off. The wavelength of maximum luminescence intensity was nearly 450 nm. The power density was about 3 mW/cm^2.

Result and discussion

SEM observation. Figure 1(a) shows a SEM image of the Pt/Ti electrode deposited by sputtering on a SiO_2 substrate. The electrodes are separated by a distance of about 100 nm. Figure 1(b) shows a typical SEM image of the MoC nanowire (top) and MoO nanowire (down) with different sizes deposited by on-demand EBID. The MoC nanowire is about 30 nm in diameter and 500 nm in total length. It is necessary to emphasize that, as in Fig. 1(b), the present EBID can produce plural nanowires in a restricted narrow region. They can be deposited with nanometer precision and predefined shapes in an arbitrary location on the electronic circuit. A schematic illustration of an arbitrary structure nanofabricated using by EBID is shown in figure 1(c). The focused electron beam was positioned on the surface of the substrate and was then moved, which resulted in the formation of a nanowire. The growth of the MoOx and MoCx nanowires follows the position of the electron beam. Moreover the shape of the nanowires can be controlled arbitrarily.

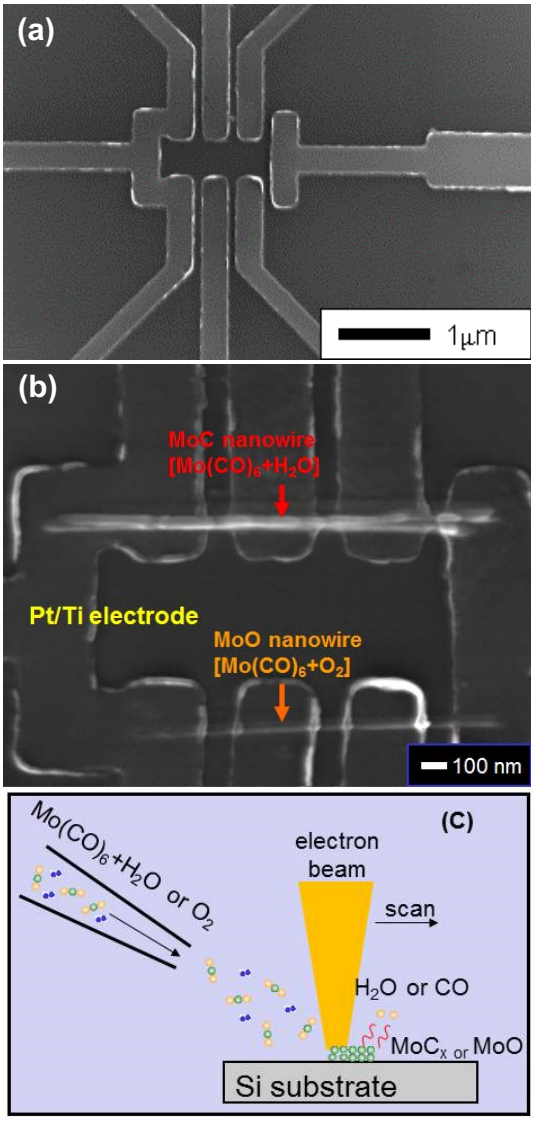

Figure 1 | (a) SEM image of Pt/Ti electrodes for two sets of a four-terminal system on a SiO substrate. (b) SEM image of Mo based nanowires prepared using $Mo(CO)_6$ gas mixed with different gases. (c) Schematic drawing of electron beam induced deposition for electrical transport measurements.

TEM and microstructural characterization. To achieve microstructural characterization without the contribution of the elements in some substrates, self-standing rods of nanometer size were also grown on an edge of platinum substrates. Details of the TEM sample procedure were reported elsewhere[10]. The nanorods were observed by transmission electron microscopy (TEM; JEOL JEM-3000F) and electron energy loss spectroscopy (EELS). Figure 2(a) shows a high-resolution transmission electron microscopy (HRTEM) image of the self-standing as-deposited nanowire prepared in $Mo(CO)_6$ gas. Both the HRTEM and Fourier-transformed images shown in the inset reveal that the structure of the specimen is amorphous. Figure 2(b) shows the EELS profile. Not only molybdenum edge but also carbon and oxygen edges are recognized. The relative ratio of these elements, Mo : O : C, is determined to be about 1.0 : 3.5 : 0.2. Although the possible equilibrium phases at room temperature are Mo, MoC_{1-x} and MoO_{3-y} compounds, x and y could not be determined at the present stage. Nonetheless, we could not detect any other elements except Mo, C and O.

Heat treatments in vacuum and in air. A bright-field TEM image and a map of element distributions of the as-deposited nanowire prepared in the $Mo(CO)_6$ gas are shown in Figs. 3(a) and 3(b), respectively. Figure 3(b) shows that Mo, C and O are distributed

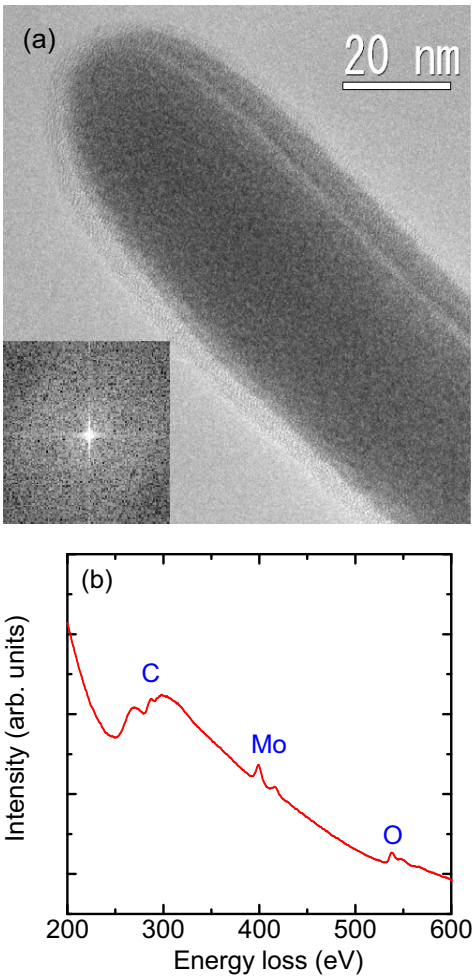

Figure 2 | (a) High-resolution TEM image of an as-deposited nanowire formed with $Mo(CO)_6$ gas. The inset shows the fast Fourier transforms of the TEM image. (b) EELS profile of the as-deposited nanowire.

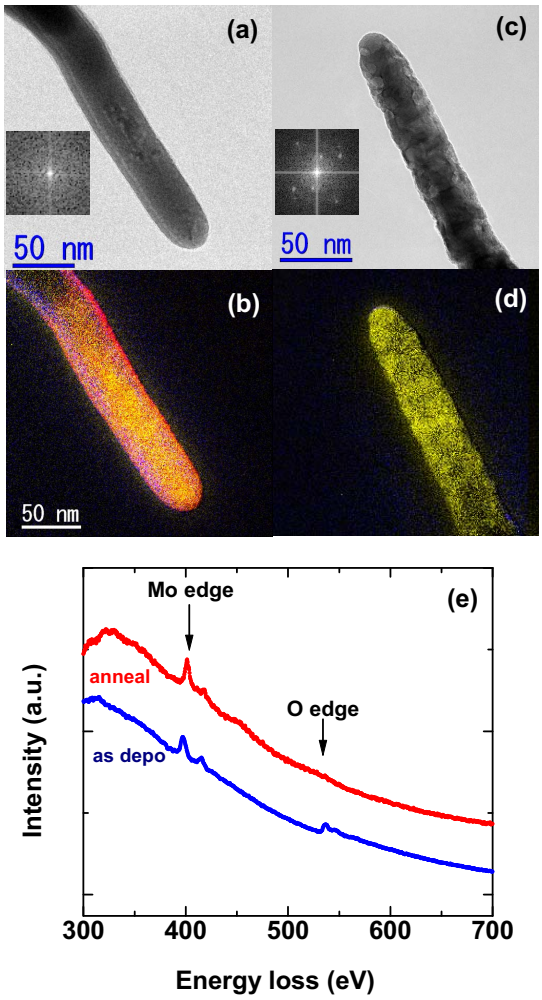

Figure 3 | (a) Bright-field TEM images and (b) map of element distributions for as-deposited nanowire prepared in the $Mo(CO)_6$ gas. (c) Bright-field TEM images and (d) map of element distributions for nanowire annealed at T=973 K for 0.5 h in vacuum. The insets show the fast Fourier transforms of the TEM images. (e) EELS profile of (—) as-deposited nanowire and (—) annealed nanowire.

homogeneously in the entire region of the as-deposited nanowire, where yellow, red and blue correspond to Mo, C and O, respectively. Figures 3(c) and 3(d) also respectively show TEM image and a map of an as-deposited nanowire annealed at T=973 K for 0.5 h in heating chamber evacuated to $\sim 10^{-6}$ Pa. During the heat treatment, the pressure in the chamber was kept below 1×10^{-5} Pa. Both insets in Figs. 3(a) and 3(c) show the Fourier-transformed images of the bright-field TEM images.

The structures of as-deposited and annealed as-deposited nanowires are amorphous and crystalline, respectively. Figure 3(e) shows the EELS profile taken at the edge of the rod of both nanowires, where carbon cannot be detected in the substrate. Although oxygen could be detected near the surface of the as-deposited nanowire, the thin oxidized surface layer disappeared after the heat treatment. Thus, we can prepare Mo nanowires by this heat treatment in vacuum. On the other hand, when nanowires are annealed in air, we can prepare highly resistive MoO_x nanowires that can serve as photodetectors.

Effects of O_2 and H_2O gas injection. Figure 4(a) shows the relationship between the atomic ratio of each element and the partial pressure ratio of O_2 gas, $O_2/[O_2 + Mo(CO)_6]$, determined by scanning TEM energy-dispersive X-ray spectroscopy (STEM-EDS). Although there is a small atomic ratio of C in the as-deposited nanowire, namely, $O_2/[O_2 + Mo(CO)_6]=0$, we cannot detect C (below 0.1 atomic ratio) for the specimens prepared at $O_2/[O_2 + Mo(CO)_6]>0.2$. The I-V characteristics and photoresponse of the MoO_x nanowire prepared at $O_2/[O_2 + Mo(CO)_6] \approx 0.4$ are shown in next section.

The relationship between the atomic ratio of each element and the partial pressure ratio of H_2O gas, $H_2O/[H_2O + Mo(CO)_6]$, is shown in Fig. 4(b). For the nanowires prepared in the mixed $Mo(CO)_6$ and H_2O gases, carbon content increases and oxygen content decreases with increasing ratio of H_2O partial pressure. Taking into account the detection accuracy of EELS of about 3–5%, it is considered that the oxygen ratio reached almost zero in the region where the partial pressure ratio is larger than 0.4. The proportions of Mo and C are constant, and the Mo and C contents were approximately 70 and 30 at.%, respectively. Of course, it is not possible to eliminate the influence of hydrogen. However, it should be noted that Mo and C elements are dominant and hydrogen is considerably little. We think that the electron beam dissociated precursor molecules by cutting Mo-CO_6, H-O, C-O, and H-C bonds, consequently nonvolatile metal parts were deposited along the electron beam scanning line, and therefore nanowire were formed. Most gaseous organic ligands were passed out of the chamber.

Electric transport properties. In this section, we will show the present experimental data for the photoresponse of the MoO_x nanowire and the marked decrease of $R(T)$ of the MoC nanowire

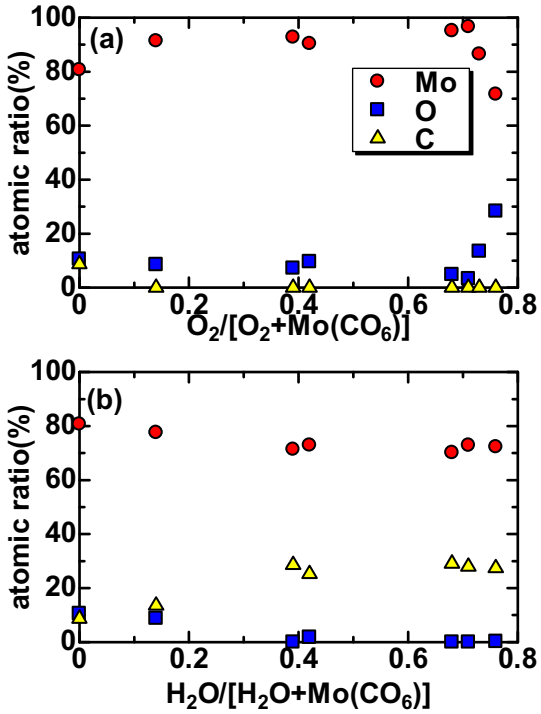

Figure 4 | Composition of deposits as a function of partial pressure ratio, using (a) mixed gas of $Mo(CO)_6$ and O_2 and (b) mixed gas of $Mo(CO)_6$ and H_2O.

near $T \approx 10$ K, suggesting superconductivity. These results are indicative of future of on-demand EBID as a dependable means of successfully fabricating functional nanodevices.

MoO_x nanowire. Figure 5(a) shows the *I-V* characteristics at $T=300$ K of the MoO_x nanowire annealed in vacuum. The linear *I-V* relation suggests that the annealed nanowire is metallic. This is consistent with the resistivity $\rho(300\ \mathrm{K})$ of this specimen being $\rho \approx 150\ \mathrm{m\Omega m}$, which is close to that of MoO_2, a metal[17]. As shown by different marks, the radiation of white light does not show any effect on conductivity.

In contrast, for the MoO_x nanowire obtained by annealing above 573 K for 2 h in air, Figs. 5(b) and 5(c) show the *I-V* characteristics and differential conductance as functions of *V* at $T=300$ K, respectively. The *I-V* relation in the dark (off state) shows a nonlinear dependence and an asymmetric behavior. As shown in Fig. 5(b), the conductance under illumination (on state) exceeds that in the dark by a factor of ≈100 in the range of $-1\ \mathrm{V} < V < 1\ \mathrm{V}$. These *I-V* characteristics are similar to those of Schottky contacts. The resistivity $\rho(300\ \mathrm{K})$ at $V \approx 0$ V is about 10 Ωm. As discussed in our previous work[18], nanowire annealed in air has a crystal structure, whereas an as-deposited nanowire has an amorphous structure. Therefore, an annealed MoO_x nanowire may have different oxidation states from an as-deposited nanowire. From the experimental result that the microscopic structure of the annealed MoO_x nanowire changes even at a low annealing temperature (~573 K), we consider that oxygen atoms can diffuse on the basis of the interstitial diffusion mechanism and the nanowire takes a different oxidation state. Therefore, it is assumed that the electrical properties of molybdenum oxide depend on oxidation state. Taking account of the well-previous known results that MoO_2 is a metallic conductor[19] and MoO_3 is a semiconductor[20], we conclude that annealing the nanowire in air efficiently enhances its oxidation. Furthermore, it is worth emphasizing the applicability of the annealed nanowire in visible optoelectronic devices. Although, we do not observed any photo-induced conductance enhancement for the as-deposited nanowires

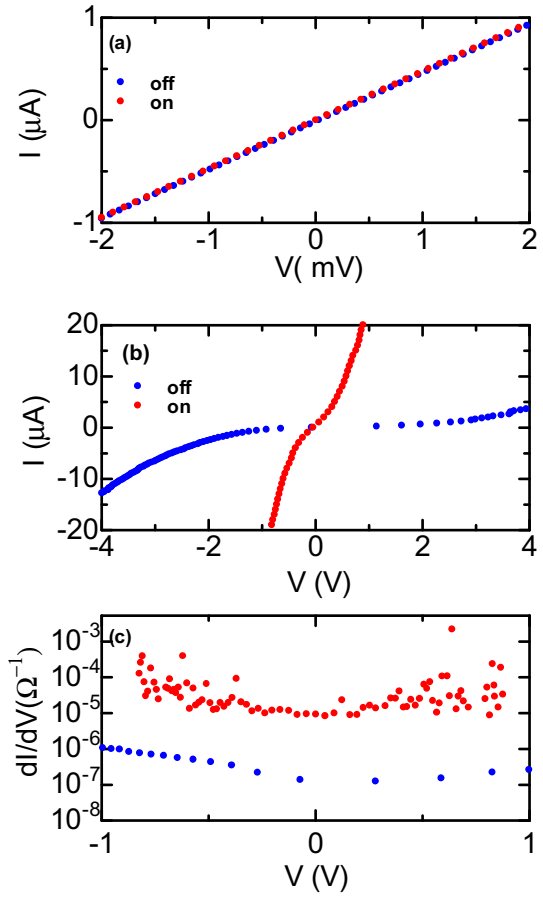

Figure 5 | *I–V* curves for (a) as-deposited nanowire formed in mixed gas of $Mo(CO)_6$ and O_2 with $O_2/[O_2 + Mo(CO)_6] > 0.2$ and (b) nano-wire annealed in air. Marks (•) and (•) show data obtained in the dark and under illumination, respectively.

even under illumination, we observed an interesting photocurrent behavior showing a change in the *I–V* curves in the case of light injection, as shown in Fig. 5(b). This result indicates that MoO_x nanowires can function as photoconductors with a high sensitivity.

Mo and MoC nanowires. Figure 6 shows the *T* dependences of ρ below ≈ 20 K for (a) a crystallized Mo nanowire and (b) an amorphous MoC (a-MoC) nanowire. ρ(T) was measured by the four-terminal method, as shown in Fig. 1. The crystallized Mo nanowire prepared by annealing the as-deposited nanowire shown in Fig. 3 is metallic, namely, its ρ decreases with decreasing *T*. On the other hand, as shown in Fig. 6(b), the $\rho(T)$ of the as-deposited MoC nanowire prepared in the mixed $Mo(CO)_6$ and H_2O gases at $H_2O/[H_2O + Mo(CO)_6] > 0.4$ shows a semiconducting transport property of $d\rho/dT < 0$ at $T > 10$ K and decreases gradually with decreasing *T*. The behavior of the ρ (*T*) at approximately $T \approx 10$ K indicates that a possibility of competition occurs between the electron localization effect and superconductivity. To the best of our knowledge, there has been no discussion yet on the superconductivity of nanowires fabricated by EBID. We expect that the present preparation technique and analysis of ρ (*T*) will contribute to the development of nanosize superconductors.

For comparison of the present data with the data of our previous investigations, we will show the $\rho(T)$ superconducting characteristics of amorphous Mo and MoC films obtained by quenched condensation (q-c) onto a substrate cooled to liquid He temperatures. We prepared amorphous superconducting Mo (99.95%) and $Mo_{75}C_{25}$ films on a substrate coated with an insulating SiO thin layer[21]. We

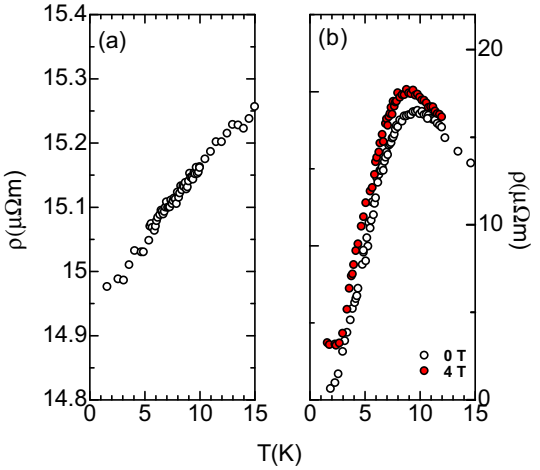

Figure 6 | $\rho(T)$ values of (a) crystalline Mo nanowire and (b) a-MoC nanowire. The magnetic field H=4 T in (b) is applied perpendicularly to the substrate.

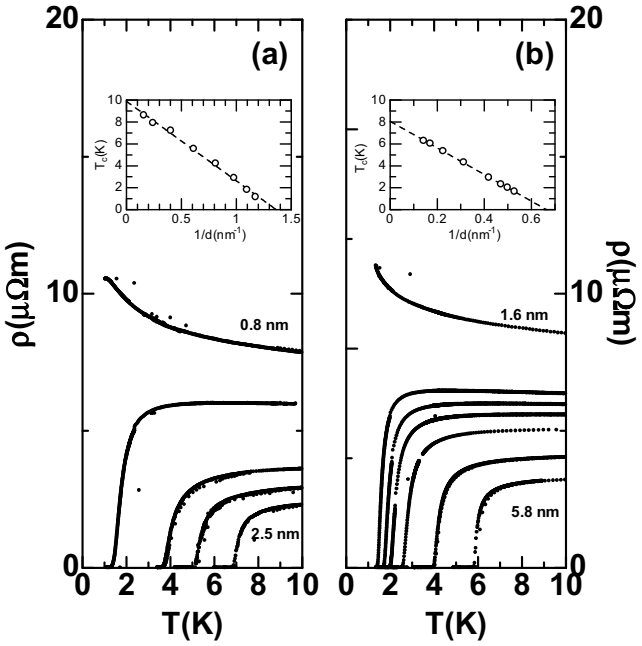

Figure 7 | $\rho(T)$ values of series of quench-condensed films on substrates with a SiO underlayer: (a) a-Mo and (b) a-MoC. Numerals denote the ranges of the film thicknesses of a-Mo and a-MoC.

measured evolution of $\rho(T)$ increasing the film thickness, *in situ*. Figures 7(a) and 7(b) show the temperature dependences of the sheet resistances $R_{sq}(T)$ of Mo and MoC films with various film thicknesses, respectively. T_c increases markedly with increasing film thickness. The $T_{c,bulk}$ values of the q-c Mo and q-c MoC films were estimated to be ≈ 9.8 K and ≈ 7.6 K, respectively, by extrapolation to the infinite film thickness, as shown in the insets. These values are substantially higher than the T_c ≈0.92 K of bulk crystalline Mo. In contrast to the q-c Mo film in Fig. 7(b), the present crystallized Mo nanowire shown in Fig. 6(a) shows no evidence of superconductivity above T = 2 K. As mentioned above, this result is consistent with the T_c of crystalline Mo being 0.92 K even in the bulk case. As for the q-c a-MoC films in Fig. 7(b), their Mo and C contents were determined by X-ray photoelectron spectroscopy to be 65 and 35 at.%, respectively, which are close to those of the present MoC nanowire, as shown in Fig. 4(b). However, it is not easy to compare the absolute value of the T_c of the present nanowire with that of the q-c a-MoC films because of the differences in dimensionality and dirtiness dependence between these specimens.

Another difference between the q-c a-MoC films and the present a-MoC nanowire is in the transition width due to the different dimensionalities used, namely, two-dimensional (2D) and one-dimensional (1D). Although it is clear that, as T decreases, the resistivity $\rho_{2D}(T)$ of the q-c films gradually decreases above T_c because of thermal fluctuations due to the Aslamazov Larkin and Maki-Thomson terms[22–24], $\rho_{2D}(T)$ decreases sharply below T_c. Note that the $\rho_{1D}(T)$ of MoC nanowire shows a gradual decrease in a wide temperature range below T_c.

Now, assuming the possibility that the present MoC nanowire is a 1D superconductor, we briefly show the result of our analysis of the $\rho_{1D}(T)$ from the viewpoint of the thermal activation phase-slip (TAPS) and quantum phase-slip (QPS) effects in 1D superconductors. As for the TAPS mechanism, several theories have been developed. Langer *et al.* derived a model that can account for phase-slip due to the thermal activation of the order parameter near T_c[25,26]. The $R(T)$ below T_c of the MoC nanowire is fitted to the expression

$$R(T)_{\mathrm{TAPS}} = \frac{\phi_0 \Omega}{k_B T/\phi_0} \exp[-\Delta F/k_B T], \qquad (1)$$

where $\phi_0 = hc/2e = 2.07 \times 10^{-15}$ Wbm^2 is the flux quantum and $\Delta F = (8\sqrt{2}/3)(H_c^2/8\pi)A\xi$ is the energy barrier, ξ is the coherence length and A is the cross-sectional area of the nanowire. $\Omega = (L/\xi)(\Delta F/k_B T)^{1/2}(1/\tau_{GL})$, L and τ_{GL} are the attempt frequency, the length of the nanowire and the Ginzburg-Landau relaxation time given by $\tau_{GL} = \pi\hbar/8k_B(T_c - T)$, respectively. When quasi particles are considered, the total resistance is given by $R = (1/R_N + 1/R_{TA})^{-1}$ as the dotted line in Fig. 8, where R_N is the normal-state resistance of a nanowire above T_c. This fitting of $R(T)$ was performed, with T_c and $\xi(0)$ as adjustable parameters. From the fitting procedure, we obtained T_c=7.2 K and $\xi(0)$ ≈ 700 nm. Note that, in this case, the obtained $\xi(0)$ markedly exceeds the values estimated from the Ginzburg-Landau theory given by

$$\xi(0) = \{(\phi_0/2\pi T_c)[|(dH_{c2}/dT)_{T\approx Tc}|]\}^{-1/2}. \qquad (2)$$

From the analysis of $\rho(T)$ at H= 0 and H=4 T in Fig. 6(b) using eq. (2), we can roughly estimate the length $\xi(0)$ ≈ 8 nm.

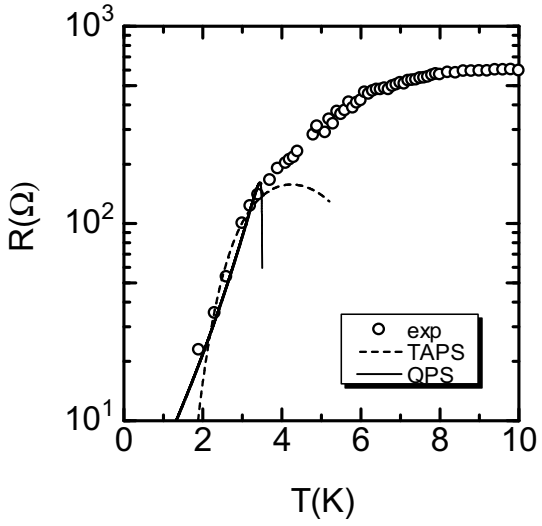

Figure 8 | Semi-log plot of R versus T for an a-MoC nanowire at H=0. Solid and dotted lines show the theories for the phase-slip behavior based on the QPS and TAPS, respectively.

As suggested by equation (1), resistance exponentially vanishes as T approaches zero. Such a strong temperature dependence of $R(T)$ for tin whiskers of 0.5 μm diameter was observed in the high temperature range of $T \leq T_c$ to confirm the theory. On the other hand, Giordano observed that thin In and PbIn wires show weaker temperature dependences of their resistances at lower temperatures[27]. To explain their experimental results, they proposed a model that takes account of the possibility of QPS through the same energy barrier ΔF. The expression for $R(T)_{QPS}$ is given by

$$R_{QPS}(T) = \alpha R_Q \left(\frac{8\sqrt{3}L}{2\pi^{\frac{5}{2}}\xi_0}\right) 0.83 \left(\frac{LR_Q}{\xi_0 R_N}\right)^{\frac{1}{2}} \left[\left(1-\frac{T}{T_C}\right)^{\frac{7}{4}} \frac{T_C}{T}\right] \exp\left[-0.83\alpha\left(\frac{LR_Q}{\xi_0 R_N}\right)\left[\left(1-\frac{T}{T_C}\right)^{1/2}\right]\right], \quad (3)$$

where $R_Q (= h/4e^2 \approx 6.45\ k\Omega)$ and R_N is the quantum resistance. Here, α is the numerical factor on the order of unity. This model is clearly recognized by the theoretical work of Golubev and Zaikin[28]. We fitted eq. (3) to the $\rho(T)$ data, using α as the fitting parameter using the length L of this nanowire and $\xi(0) \approx 8$ nm determined from equation (2). The solid line in Fig. 8 was calculated using equation (3) with $T_c \approx 4$ K and $\alpha \approx 0.055$. Although the present data are unfortunately restricted above 2 K, we consider that the theory is in agreement with the experimental data with only the parameter α and a reasonable $\xi(0)$. As for the prefactor $\alpha < 1$ determined from the fitting procedure being less than the theoretical suggestion, further investigation is necessary.

Conclusion

We have fabricated MoO_x and MoC nanowires prepared on a SiO_2 substrate by the on-demand EBID using a $Mo(CO)_6$ precursor with O_2 and H_2O, respectively. The MoO_x nanowire prepared by annealing an as-deposited nanowire in air shows a semiconducting transport characteristic and a photodetecting property, showing potential as an optical switch. We think that the optimization of nanowire composition can improve the optical sensitivity and photoresponse of the nanowire. On the other hand, a-MoC nanowires show evidence consist with a superconducting resistive transition. The $\rho(T)$ in the temperatures below T_c can be explained by the quantum phase-slip model. The above wires can be fabricated into any shape with nanosize and high spatial accuracy.

1. Mourik, V. *et al.* Signature of Majorana fermions in hybrids superconductor-semiconductor nanowire devices. *Science* **336**, 1003–1007 (2012).
2. Nadj-Perge, S., Frolov, S. M., Bakkers, E. P. A. M. & Kouwenhoven, L. P. Spin-orbit qubits in a semiconductor nanowire. *Nature* **468**, 7237 (2010).
3. Akimov, A. V. *et al.* Generation of single optical plasmons in metallic nanowires coupled to quantum dots. *Nature* **450**, 402–406 (2007).
4. Wang, J. *et al.* Interplay between superconductivity and ferromagnetism in crystal nanowires. *Nat. Phys.* **6**, 389–394 (2010).
5. Sadki, E. S., Ooi, S. & Hirata, K. Focused-ion-beam deposition of superconducting nanowires. *Appl. Phys. Lett.* **64**, 6206–6208 (2004).
6. Van Drop, W. F., van Someren, B., Hagen, C. W. & Kruit, P. Approaching the resolution limit of nanometer-scale electron beam-induced deposition. *Nano Lett.* **5**, 1303 (2005).
7. Utke, I. *et al.* Cross section investigations of compositions and sub-structures of tips obtained by focused electron beam induced deposition. *Adv. Eng. Mater.* **7**, 323 (2005).
8. Koops, H. W. P., Kaya, A. & Weber, M. Fabrication and characterization of platinum nanocrystalline material grown by electron-beam induced deposition. *J. Vac. Sci. Technol. B* **13**, 2400 (1995).
9. Shimojo, M. *et al.* Selective growth and characterization of nanostructures with transmission electron microscopes. *Appl. Surf. Sci.* **241**, 56–60 (2005).
10. Shimojo, M., Takeguchi, M. & Furuya, K. Formation of crystalline iron oxide nanostructures by electron beam-induced deposition at room temperature. *Nanotechnology* **17**, 3637–3640 (2006).
11. Gazzadi, G. C., Frabboni, S. & Menozzi, C. Suspended nanostructrues grown by electron beam-induced deposition on Pt and TEOS precursors. *Nanotechnology* **18**, 445709 (2007).
12. Utke, I., Hoffmann, P., Berger, R. & Scandella, L. High-resolution magnetic Co supertips grown by a focused electron beam. *Appl. Phys. Lett.* **80**, 4792–4794 (2002).
13. Luxmoore, I. *et al.* Low temperature electrical characterization of tungsten nanowires fabricated by electron and ion beam induced chemical vapour deposition. *Thin Solid films* **515**, 6791–6797 (2007).
14. Taurino, A. M. *et al.* Synthesis, electrical characterization, nad gas sensing properties of molybdenum oxide nanorods. *Appl. Phys. Lett.* **88**, 152111 (2006).
15. Zhang, W., Desikan, A. & Oyama, S. T. Effect of support in ethanol oxidation on molybdenum oxide. *J. Phys. Chem.* **99**, 14468–1447 (1995).
16. Ohfuji, S. C., Hashimoto, C., Amazawa, T. & Murota, J. Oxygen-doped molybdenum films for MOS gate application. *J. Electrochem. Soc.* **131**, 446–450 (1984).
17. Li, Z. *et al.* Investigation on molybdenum and its conductive oxides as p-type metal gate candidates. *Journal of the Electrochemical Society* **155**, H481–H484 (2008).
18. Makise, K., Mitsuishi, K., Shimojo, M. & Furuya, K. A nanosized photodetector fabricated by electron-beam-induced deposition. *Nanotechnology* **20**, 425305 (2009).
19. Dissanayake, M. A. K. L. & Chase, L. L. Optical properties of CrO_2, MoO_2, and WO_2 in the range 0.2-6 eV. *Phys. Rev. B* **18**, 6872 (1978).
20. Julien, C., Khelfa, A., Hussain, O. M. & Nazri, G. A. Synthesis and characterization of flash-evaporated MoO_3 thin-films. *J. Cryst. Growth* **156**, 235 (1995).
21. Hirakawa, A., Makise, K., Kawaguti, T. & Shinozaki, B. Thickness-tuned superconductor-insulator transitions in quench-condensed Mo and MoRu films. *J. Phys. Condens. Matter* **20**, 485206 (2008).
22. Aslamazov, L. G. & Larkin, A. L. Influence of fluctuation pairing of electrons on conductivity on normal metal. *Phys. Lett. A* **26**, 238 (1968).
23. Maki, K. Critical fluctuation of order parameter in type-II superconductors. *Prog. Theor. Phys.* **39**, (1968).
24. Thompson, R. S. Microwave, flux flow, and fluctuation resistance of dirty type-II superconductors. *Phys. Rev. B* **1**, 327 (1970).
25. Langer, J. S. & Ambegaokar, V. Intrinsic resistive transition in narrow superconducting channels. *Phys. Rev.* **164**, 498 (1967).
26. McCumber, D. E. & Halperin, B. I. Time scale of intrinsic resistive fluctuations in thin superconducting nanowires. *Phy. Rev. B* **1**, 1054 (1970).
27. Giordano, N. Superconductivity and dissipation in small-diameter Pb-In wires. *Phys. Rev. B* **43**, 160 (1991).
28. Golubev, D. S. & Zaikin, A. D. Quantum tunneling of the order parameter in superconducting nanowire. *Phys. Rev. B* **64**, 014504 (2001).

Author contributions

K.M. performed most of the experiments and analyzed the data. M.S. contributed to the growth of nanowires. K. Mitsuishi contributed to the STEM images. All of the text of the paper was written jointly K.M. and B.S.

Additional information

Competing financial interests: The authors declare no competing financial interests.

How to cite this article: Makise, K., Mitsuishi, K., Shimojo, M. & Shinozaki, B. Microstructural analysis and Transport Properties of MoO and MoC nanostructures prepared by focused electron beam-induced deposition. *Sci. Rep.* **4**, 5740; DOI:10.1038/srep05740 (2014).